



Quasi-in-situ sizing of nanoparticles by laser-induced incandescence during the floating chemical vapor deposition synthesis of carbon nanotubes

Yiguo Xu¹ · Yang Ma² · Delong He¹ · Hanlu Zhang¹ · Laurent Zimmer³ · Anthony Dichiara⁴ · Paul Haghi-Ashtiani¹ · Jinbo Bai¹

Received: 21 February 2019 / Accepted: 24 April 2019 / Published online: 6 May 2019
© Springer-Verlag GmbH Germany, part of Springer Nature 2019

Abstract

In this study, laser-induced incandescence (LII) diagnostic technique was applied for iron-based nanoparticle (NP) sizing during the floating chemical vapor deposition (CVD) synthesis of carbon nanotubes (CNTs). Transmission electron microscopy (TEM) was used to characterize the nature and size of NPs. The LII signal was simulated by taking into account the carbon-encapsulated iron NP density, heat capacity, size distribution, etc. A detailed sensitivity and uncertainty of the key parameters on the evaluated particle size for this model has also been estimated. Using the developed approach, the evolution of NPs in the gas phase along the reactor axis was investigated at 650, 750 and 850 °C. It was found that the evaluated sizes from LII signals were in good agreement with the ones obtained by TEM measurements. The NP size is highly dependent on the temperature under the studied conditions but it does not show obvious difference along the reactor axis. This study reveals an important LII application prospect to understand the catalyst particle behaviors for better control over CNT growth during the floating CVD process.

Yiguo Xu and Yang Ma contributed equally to this work.

This article is part of the topical collection “Laser-Induced Incandescence”, guest edited by Klaus Peter Geigle and Stefan Will.

Electronic supplementary material The online version of this article (<https://doi.org/10.1007/s00340-019-7201-4>) contains supplementary material, which is available to authorized users.

✉ Delong He
delong.he@ecp.fr

✉ Jinbo Bai
jinbo.bai@ecp.fr

¹ Laboratoire MSSMat, CNRS UMR 8579, CentraleSupélec, Université Paris-Saclay, 8-10 rue Joliot-Curie, 91190 Gif-sur-Yvette, France

² Key Laboratory of Aerospace Advanced Materials and Performance of Ministry of Education, School of Materials Science and Engineering, Beihang University, Beijing 100191, China

³ Laboratoire EM2C, CNRS UPR 288, CentraleSupélec, Université Paris-Saclay, 8-10 rue Joliot-Curie, 91190 Gif-sur-Yvette, France

⁴ School of Environmental and Forest Sciences (SEFS), University of Washington, 4000 15th Ave NE, Seattle, WA 98195, USA

1 Introduction

Due to their extraordinary intrinsic properties, CNTs have made themselves very attractive and can be potentially used in various fields such as energy storage [1, 2], environmental remediation [3, 4] and structural composites [5]. These exhibited properties in mechanics, electrics and thermotics are strongly related to their morphology, length, diameter, wall numbers and crystallinity [6]. However, the production of CNTs with specific and uniform properties in large amount still remains a challenge and several post-treatment steps are usually demanded [7]. Among all the different synthesis methods, floating catalyst CVD (FCCVD) approach, where both carbon feedstock(s) and catalyst precursor(s) are simultaneously fed into the reactor, allows low cost, high quality and continuous production for industrial purposes [8, 9]. Ferrocene is commonly used as the catalyst precursor due to its low cost and non-toxicity. Even though the CNT synthesis by FCCVD always occurs on a substrate like quartz plate or microspherical alumina particle, many researchers proposed that the catalytic NPs formation also takes place in the gas phase by homogeneous nucleation [10–13], because the catalytic NPs originate from decomposition

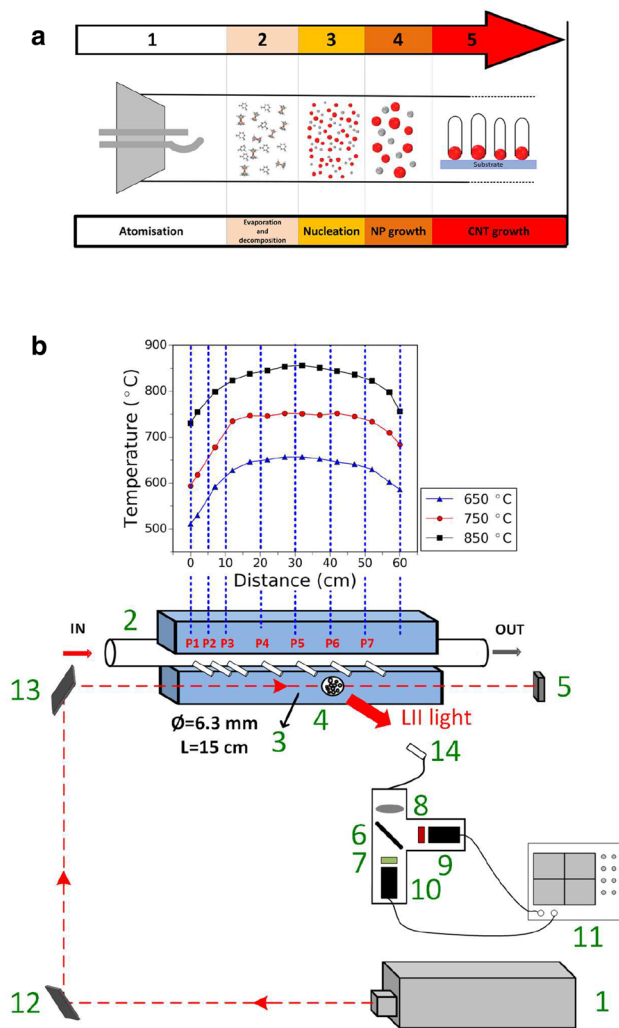


Fig. 1 **a** Schematic illustration of CNT synthesis in a FCCVD reactor. **b** Experimental setup for LII measurements. 1. Nd:YAG pulsed laser (10 Hz, 1064 nm). 2. The stainless steel CVD reactor. 3. Small open-ended tubes installed at different positions along the reactor (P1–P7). 4. Area containing NPs (outlet of the small tube). 5. Laser energy meter. 6. 550-nm Dichroic shortpass filter. (7, 8). Bandpass filter 492 and 694 nm. (9, 10) Two PMTs. 11. Oscilloscope. (12, 13). Reflection mirror. 14. Optic fiber detector

of ferrocene in the gas phase, as depicted in Fig. 1a. CNT growth precedes through several processes, such as, the NP nucleation and the following diffusion, precipitation of decomposed carbon on the catalytic NPs. In practical, all the processes may occur simultaneously at the same region in the reactor. It has been believed that the catalyst NP size and nature have a significant effect on the control of the CNT morphology, such as CNT diameter [14] as well as their chirality [15, 16]. Therefore, controlling the formation of iron-based catalyst NPs is highly desired for high-quality CNT synthesis at a large scale. To achieve an in-depth understanding of the catalytic NP formation mechanism, it is reasonable to develop an

in-situ diagnostic technique to trace the catalyst evolution and study the performance of these catalysts during the FCCVD process.

LII phenomenon occurs when a high-energy pulsed laser beam encounters particles like carbonaceous soot or metallic particles. When particles are heated up by a pulsed laser of ~ 10 ns duration, their temperature increases to ~ 4000 K immediately for laser intensities of 1×10^7 W/cm² or greater [17]. Meanwhile, the particles lose energy by heat transfer mechanisms such as conduction, radiation, evaporation, oxidation, etc., among which thermal radiation leads to the LII emission. The research on LII was first outlined by Weeks and Duley [18]. It was found that the aerosol particles generated from sub-micron powders of carbon black and alumina released a momentary emission of light when heated by TEA CO₂ laser pulses. The spectrum of this emission related to the particle size. In 1977, Eckbreth found several interferences during the Raman scattering experiments, which were identified to be laser-modulated particulate incandescence [19]. They also proposed an analytical model to describe this process. The real pioneer of LII technique is Melton. In 1984, Melton improved the equations governing the laser heating and vaporization of particles [20]. This work exploited the potentiality of LII as a powerful diagnostic tool for soot concentration measurement and particle sizing. A time-resolved variant of LII (TiRe-LII) was introduced to allow particle sizing by recording the time-dependent particle emissions during particle cooling after the laser heating by Roth [21, 22] and Will [23]. In 2004, Bladh extended the theoretical model for TiRe-LII to include particle-size distributions and different spatial distributions of the laser energy [24]. In the past decades, LII had undergone significant developments. Following the earlier modeling work of Weeks and Duley [18], different detailed models were developed to serve as means to extend LII technique to a wider variety of conditions, including high pressures and low temperatures [25–30]. In 2002, Vander Wal et al. first applied LII to study the CNT flame synthesis [31]. Snelling and coworkers developed the auto-compensating LII, henceforth LII technique can achieve a quantitative measurement of volume fraction without further calibration process using another soot measurement technique [32]. The early experiments about LII focus on soot size measurements [20, 23, 33]. Due to its non-intrusive, real-time and in-situ nature, it has recently been spread to a variety of sources, such as Cu [34], Mo [35–37], Ag [22], W [38], Ti [39], Fe [39–47], and Fe–C binary NPs [48, 49]. LII has proven to be a powerful tool for particle concentration and primary particle-size measurement, and was used in a wide range of applications, such as combustion [50–52], particle synthesis [34, 53] and environment [54–58]. However, LII technique has rarely been applied for catalytic NP sizing during CNT synthesis. The mechanistic investigation of carbon

nanotube formation was examined by Cau et al. within the framework of laser vaporization by combining LII and laser-induced fluorescence (LIF) [59]. Recently, Yatom et al. also conducted LII measurements in the carbon arc discharge for synthesis of CNTs [60]. However, the synthesis of carbon nanotube by laser vaporization and carbon arc discharge is different from CNT growth by floating catalyst CVD.

In this study, the LII technique is applied for characterizing the NP sizes during the FCCVD synthesis of CNTs. The typical equipment used in FCCVD is a horizontal quartz tube heated by an electric furnace. However, in this situation, the NPs are also deposited on the inner wall of the reactor and may contribute to the LII signal, which prevent the response of the floating NPs from being collected by the detector located outside the reactor. To avoid the effect of the deposited NPs on the LII signals, a stainless steel reactor with seven 15-cm-long stainless steel open-ended tubes (6.3 mm in diameter) welded perpendicularly to the reactor axis was designed and the gas exhaust was probed by LII at the end of each 15-cm-long tubes. Then, we conducted a validation experiment inside the reactor, where a copper grid with lacey carbon films was placed into the tube furnace. This comparative study revealed that there are no statistical differences in size and structure between the NPs inside the reactor and those collected at the location where the LII signal was probed. Furthermore, the results obtained by LII sizing were compared with TEM observation. The good agreement between the NP sizes estimated by both LII and TEM demonstrates the validity of this approach. Using this approach, the evolution of NPs in the gas phase along the reactor axis was investigated at different temperatures. These results contribute to analyze potential relations between the floating NPs and the CNTs on the substrate which were barely discussed caused by the lack of a proper method, revealing the great LII application prospect for the FCCVD CNT growth mechanism research.

2 Experimental section

The experimental setup depicted in Fig. 1b comprises a 120-cm-long stainless steel reactor (45 mm in diameter) heated by a horizontal electrical furnace (Carbolite). The reactor was opened at seven positions using 15-cm-long stainless steel tubes (6.3 mm in diameter) welded perpendicularly to the reactor axis to provide optical access to the reactive atmosphere for LII analysis [61]. No obvious size and structure change of NPs were observed from inside of the reactor to the outlet of the small tubes. The CVD process was carried out at 650, 750 and 850 °C under argon atmosphere in the presence of hydrogen. Acetylene was also introduced in the system to serve as carbon source [62, 63]. Gas flows were adjusted using digital mass

flow controllers (Bronkhorst) and the total flow rate was kept constant at 1 L/min (0.78 L/min Ar, 0.20 L/min H₂, 0.02 L/min C₂H₂). During the CVD process, a solution of ortho-xylene (98.5% Alfa Aesar) containing dissolved ferrocene (0.05 g/mL) was injected in the form of a spray at a rate of 0.2 mL/min using a syringe pump equipped with a liquid flow meter (Razel Science, R99-E) [64, 65].

The gas exhaust was probed by LII at the end of each 15-cm-long stainless steel open-ended tubes, as shown in Fig. 1b. The LII signals were generated using a pulsed Nd:YAG laser (Excel, Surelite II-10), which delivered 1064-nm emissions with 7-ns pulse duration and 2-Hz repetition rate. The non-focalized laser beams had a diameter of 7 mm and the laser fluence was monitored using an energy meter (Gentec, UP19K-15S-VM-D0) at different Q-switch values. The laser beams were directed along the CVD reactor so that the excitation of the floating particles occurred at the outlet of each open-ended tubes. The incandescence signals were collected at different positions along the reactor using an optical fiber facing each one of the open-ended tubes. The detection was arranged perpendicular to the excitation axis to minimize Rayleigh scattering. A beam splitter divided the collected particle radiation into two beams, which were arranged perpendicular to each other. Narrow band-pass filters with the center wavelengths of 492 ± 10 nm and 694 ± 10 nm were placed in each beam to limit the radiation to a narrow spectral range. The radiations were converted into electrical signals using two identical high-speed photomultipliers (Hamamatsu, H10721-20) equipped with external amplifiers (Hamamatsu, C5594-44). The signals were digitized and recorded by a 2-GHz digital storage oscilloscope (Lecroy, Wavejet 354A). For particle-size evaluation, the measured LII signal was fitted by calculated curves obtained by variation of count median diameter (CMD) and standard deviation σ_g . A least-squares method by Levenberg and Marquardt was used for curve fitting [66].

For comparison purposes, the samples of the floating particles were collected at the outlet of each open-ended tube. Sampling was conducted by introducing copper grids at the positions where the LII signals were recorded. The copper grids were withdrawn after being exposed to the gas outlet for five seconds and used for TEM observation. TEM was performed using a FEI Titan instrument equipped with a probe-corrected condenser operating at 200 kV. The histogram of NP distribution was determined by counting and sizing the primary particles from several TEM images. The histogram was fitted by a lognormal size distribution using a least-squares method and CMD as well as standard deviation can be obtained. Under each experimental condition, more than 100 particles were used for a statistic analysis.

3 Results and discussions

The measurements were based on the model described by Eremin et al. [48, 49, 67]. The detail description of the model and the procedure of determination of key parameters are demonstrated in the supplementary file. After determination of the key parameter in the LII model, the measured LII signals can be evaluated by fitting cooling curves to the experimental profiles under variation of the particle size. The representing LII signal and the best fit curve of calculated LII signal are presented in Fig. 2. It was found that the LII result is in good agreement with TEM measurements. As discussed in recent works [40, 42, 48, 49, 68], variations in the assumed properties and the experimental conditions can cause errors of the evaluated particle sizes. Therefore, the sensitivity and uncertainty of the key parameters on the evaluated particle size for our LII model were estimated. In the present study, seven key parameters, NP density ρ_p , NP heat capacity c_p , thermal accommodation coefficient (TAC) α_T , the ratio of the heat capacities of the gas γ , the molecular weight of ambient gas μ_g , the gas temperature T_g and the heat-up temperature T_0^p were taken into account. The values of α_T , NP density ρ_p and NP heat capacity c_p may be changed depending on the carbon shell structure. The uncertainty of the NP density ρ_p depends on the Fe/C mass ratio in particles. According to the TEM results, in the case of Fe/C mass ratio 1:1, the uncertainty of the NP density is between -38% and 5% . While in the case of Fe/C mass ratio 5:1, the uncertainty of NP density is ranging from -13% to 5% . The carbon shell structure has a more profound influence on the NP heat capacity. For a NP with a Fe/C mass ratio 1:1, the maximum possible uncertainty of the NP heat

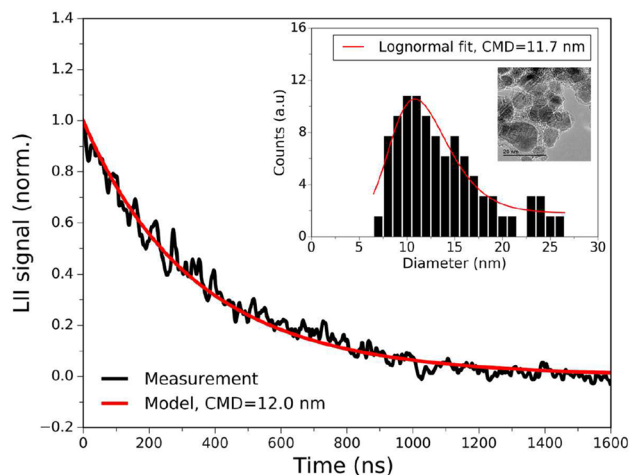
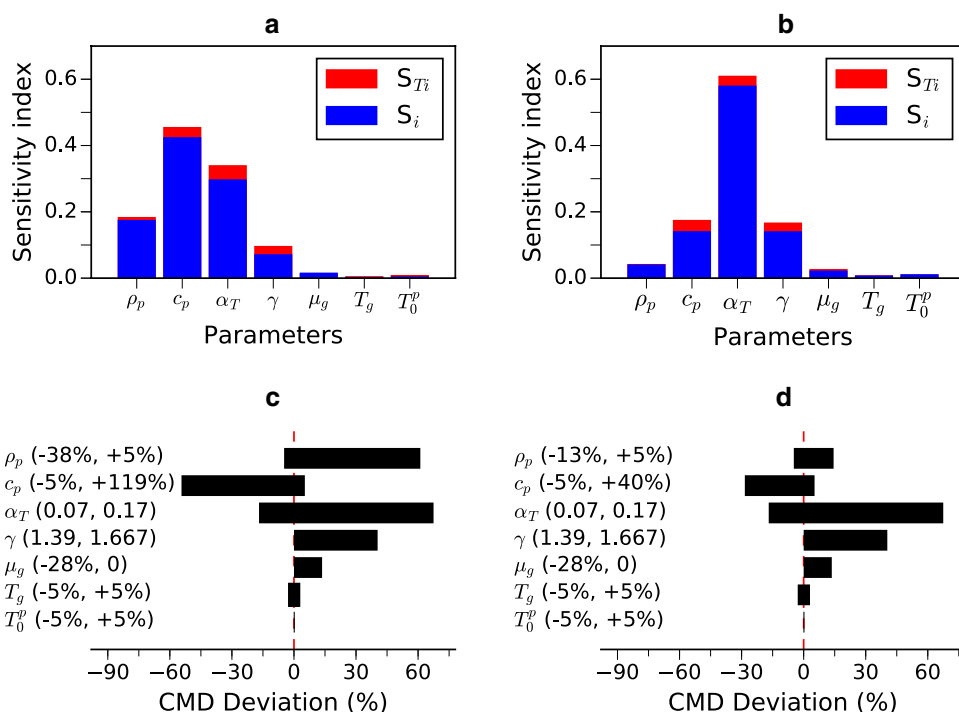


Fig. 2 Measured LII signal of NPs at the center of the reactor P5 at 850 °C in the gas phase and the best fit curve of the calculated LII signal

capacity reaches $+119\%$, which is the difference between the pure iron heat capacity value and the value for Fe/C mass ratio 1:1. It should be noted that only when all the NPs exhibit a core-shell structure with a Fe/C mass ratio 1:1, the maximum uncertainty of the NP heat capacity can reach. But according to TEM observations, the Fe/C mass ratio should be between 1:1 and 1:0. So, the uncertainty of the NP heat capacity always is smaller than $+119\%$. The value of α_T is determined by comparing the LII measurements with TEM results; hence, the real uncertainty of α_T can not be estimated. Since the differences of normalized χ^2 for α_T from 0.07 to 0.17 are very small during the two-parameter data-fit procedure (Figure S3b), the possible value of α_T is from 0.07 to 0.17. The molecular weight of ambient gas μ_g and the ratio of the heat capacities of the gas γ are related to the gas composition. The gas composition will change according to the CVD conditions. μ_g can be in the range of 28.74 (for air) to 39.39 (for argon). While, γ is ranging from 1.39 (for air) to 1.667 (for argon). The deviation of the gas temperature T_g and the heat-up temperature T_0^p are set to be $\pm 5\%$.

In the present study, Sobol's method was used to perform a detailed sensitivity analysis for our LII model by considering each parameter's individual contribution (the first-order index S_i) and the total contribution (the total-order index S_{Ti}) [69–72]. The greater the sensitivity indices are, the more critical parameters are for the model. An input factor will be considered to be important, if it explains more than $1/k$ (k is the number of the estimated parameter) of the output variance. For a given factor, a notable difference between S_{Ti} and S_i flags an important role of interactions for that factor in the output. A detailed sensitivity analysis of these influences ($\rho_p, c_p, \alpha_T, \gamma, \mu_g, T_g, T_0^p$) on the evaluated particle size for our model is presented in Fig. 3a, b. Results show that the relative sensitivity is related to the Fe/C mass ratio in the NPs. In the case of NPs with Fe/C mass ratio 1:1, c_p is the most important parameter. It explains 45.3% of the output variance. Followed by α_T and ρ_p , the total-order index of α_T and ρ_p are 0.338 and 0.182, both larger than $1/k = 0.143$. Thus, α_T and ρ_p are also important variables. Furthermore, all the input factors explain 97.8% of the output variance singly. The small difference between the total-order index and the first-order index of each parameters stands for the weak interactions between the parameters, which proves their independence. For NPs with a Fe/C mass ratio 5:1, the Sobol sensitivity index of ρ_p and c_p are 0.04 and 0.173, respectively. It indicates that ρ_p and c_p become less important with the increase in the Fe/C mass ratio. More attention should be paid to the parameter α_T in the experimental application since it becomes the most important parameter, accounting for 85.6% of the variance of the response variable. The sum of the first-order index reaches 0.93, which means that the variance of the response variable can be well explained by the uncertainty from the individual parameters.

Fig. 3 The first-order S_i and the total-order S_{T_i} Sobol sensitivity index of the main parameters in the LII model at the Fe/C mass ratio **a** 1:1 and **b** 5:1. Uncertainties in particle sizing by LII at the Fe/C mass ratio **c** 1:1 and **d** 5:1



The uncertainty of the particle size resulted from the deviation of the key parameters is also presented in Fig. 3c, d. We can clearly see that the uncertainty of the particle size caused by the ρ_p and c_p strongly depends on the Fe/C mass ratio of NPs. The possible deviation of the particle size for a NP with a Fe/C mass ratio 1:1 caused by the ρ_p and c_p is 61.1% and -54.4% . But for a NP with a Fe/C mass ratio 5:1, the uncertainty of the particle size caused by ρ_p and c_p decrease to -28.4% and 14.4% . Furthermore, among all the parameters, ρ_p , c_p , α_T , γ exhibit strong influences on the calculated particle diameter. The maximum deviation reaches 67% when $\alpha_T = 0.17$ was chosen in the present model. While, the T_0^p has a very weak influence on the evaluated particle diameter. $\pm 5\%$ deviation in the T_0^p only cause 0.39% and -0.14% uncertainty on the resulted particle diameter.

The mean size evolution of NPs in the gas phase as a function of the CVD duration was investigated by LII measurements at temperatures 650, 750 and 850 °C. It is found that temperature exhibits a pronounced effect on NP formation in the gas phase. No LII signals were detected at 650 °C at all positions along the reactor. LII signals were detected successfully at 750 and 850 °C. Figure 4 shows the mean size evolution of NPs in the gas phase at the center of the reactor as a function of the CVD duration. The CMD of NPs is almost constant in all 60 min at both 750 and 850 °C. It means that the system reaches an equilibrium state during the FCCVD process with the continuous injection of ferrocene and carbon sources. Furthermore, the evaluated CMD of NPs in the gas phase by LII at 750 and 850 °C is about 5.1 and 12.5 nm in all the time, respectively. The corresponding

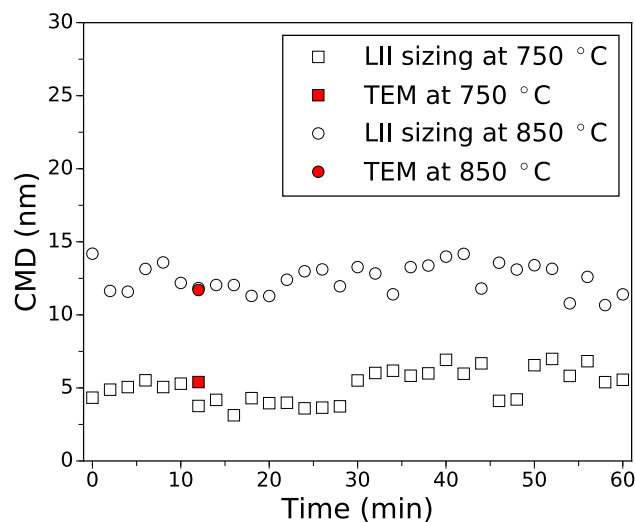


Fig. 4 NP size evolution in the gas phase at the center of the reactor as a function of CVD duration

TEM image and size distribution of NPs obtained at 750 and 850 °C with CVD duration of 12 min are depicted in Figure S6 and in Fig. 2. It can be seen that the NP size is about 5.9 and 11.7 nm by TEM measurements. These results suggest that the evaluated CMD by LII is in good agreement with the one by TEM measurements and the CMD of NPs greatly increases with the temperature increasing from 750 to 850 °C.

The NP size at different position along the reactor axis at 850 °C was also evaluated by LII measurements. At P1,

no LII signals were detected. At P2 very weak LII signals can be detected. But the detected LII signals are too weak to be analyzed for particle sizing, indicating that very few NP nucleation takes place in the gas phase at P2. From P3 to P7, we can detect strong LII signals. Therefore, the NP size from P3 to P7 can be evaluated, which is presented in Fig. 5. The corresponding TEM images and size distribution of NPs are also presented in Figure S7 and Figure S8. The NP size at position P3, P4, P5, P6 and P7 obtained by LII sizing are 10.7, 10.3, 12.5, 12.2 and 11.0 nm, respectively. In previous works, computational fluid dynamics (CFD) simulations were implemented to describe NP nucleation process [73–75]. These simulations predicted that iron NP size will increase along the reactor axis. However, in the present study, the evaluated NP size does not show obvious difference from P3 to P7. The NP size almost keep constant along the reactor. Furthermore, it is well known that highly dense CNTs can synthesize successfully at the 650 °C on the substrate at the same CVD conditions [61, 76], but at 650 °C no NPs were detected in the gas phase. It is emphasized that no CNTs were found in CVD samples collected in the gas phase by TEM analysis (Figure S1) and the CVD samples were identified to be carbon-encapsulated iron NPs. Their size is far from that on the substrate as observed in our previous study [61]. Because of the graphite layer, the carbon-encapsulated iron NPs are thermally stable, they cannot directly contribute to the CNT growth in the gas phase or coalesce on the substrate to form large NPs for the CNT growth on the substrate. Based on the above discussions, it can be deduced that iron NPs on the substrate must nucleate by another mechanism. It is hypothesized that iron NPs form in the gas phase by homogeneous nucleation when the iron partial pressure is higher than its saturated vapor pressure.

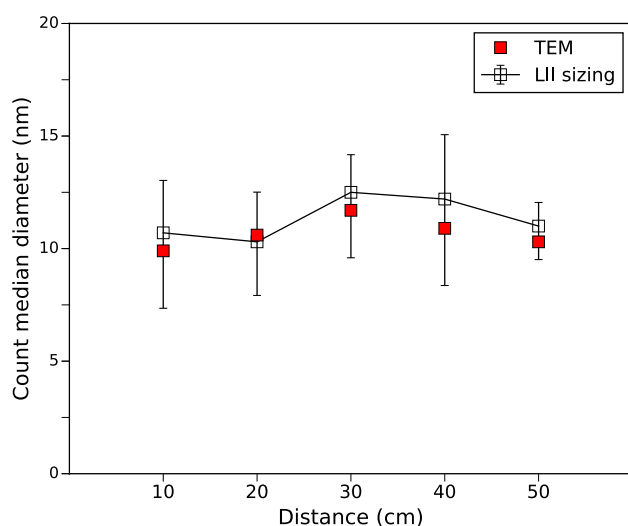


Fig. 5 NP size evolution in the gas phase at different positions in the CVD reactor at 850 °C

Since the direct bond cleavage pyrolysis of hydrocarbon carbon only happens at temperature much higher than 850 °C [49], it can be concluded that carbon atoms mainly come from the catalytic decomposition of hydrocarbon on the iron NP surface. They dissolve into iron NPs and then precipitate from iron NP surface. Once carbon atoms aggregate to a certain amount, the growth of iron NP will terminate due to the encapsulation of the carbon layers. At high temperature, fast decomposition of ferrocene will promote the NP nucleation and coalescence, finally leading to larger NPs. In addition, NPs in the gas phase are finally encapsulated by graphite layers, and they do not contribute to CNT growth on the substrate. By contrast, NPs on the substrate form by heterogeneous nucleation. The substrate plays a key role in promoting the NP nucleation, which results in much larger iron NP than those in the gas phase. Thus, NPs formed on the substrate can be used as the catalysts for the CNT growth in the studied conditions.

4 Conclusion

In summary, LII diagnostic technique was applied for NP sizing during the CVD synthesis of CNTs in this study. TEM shows that NPs in the gas phase exhibit a core-shell structure with an iron core and carbon shell. Therefore, the procedure of calculating the theoretical LII signal was developed for the carbon-encapsulated iron NP. A detailed sensitivity and uncertainty of the key parameters on the evaluated particle size for this model were estimated. Results show a strong dependence of the sensitivity and uncertainty on the structure of NPs. In the case of the NPs with Fe/C mass ratio 1:1, according to Sobol sensitivity index, c_p , α_T and ρ_p are important parameters. The possible deviation caused by the ρ_p and c_p is 61.1% and -54.4%, respectively. While for the NPs with Fe/C mass ratio 5:1, c_p and ρ_p become less important. α_T is the most important parameter. The uncertainty of the particle size resulted from ρ_p and c_p also decrease to -28.4% and 14.4%, respectively. Using the developed approach, the evolution of NPs in the gas phase along the reactor axis was investigated at 650, 750 and 850 °C. The evaluated size by LII is in good agreement with the one obtained by TEM measurements. The NP size is highly dependent on the temperature under the studied conditions but it does not show obvious difference along the reactor axis. According to these results and discussions, it is reasonable to believe that NPs form in the gas phase originated by homogeneous nucleation, and they do not directly contribute to CNT growth taking place on the substrate surface.

This study demonstrates that the LII technique is a useful tool to trace the NP evolution during the floating CVD process. However, LII is limited to the detection of NPs with the size larger than several nm. The whole NP nucleation

concerns some fundamental processes, such as decomposition of ferrocene and atoms collision. Thus, to investigate the early stage of NP nucleation, other diagnostic techniques, such as LIF [59, 77–79] or Raman, are also highly desired. The investigation of iron atoms and carbon radicals in the gas phase would confirm the NP nucleation mechanism. Furthermore, the particle agglomerates are observed in the TEM images. So, a planar LII approach could be expected for further modification of the furnace, to achieve a more precise visualization of the NPs coagulation regions [80].

Acknowledgements This work was carried out within the MATMECA consortium and supported by the ANR under contract number ANR-10-EQPX-37. Y. Xu gratefully acknowledges the financial support of China Scholarship Council (CSC). The authors thank Mr. Xiangtuo Chen for the helpful discussion.

References

1. A.B. Dichiaro, J. Yuan, S. Yao, A. Sylvestre, L. Zimmer, J. Bai, J. Mater. Chem. A **2**(21), 7980 (2014)
2. Q. Zhang, J.Q. Huang, W.Z. Qian, Y.Y. Zhang, F. Wei, Small **9**(8), 1237 (2013)
3. A.B. Dichiaro, S.F. Harlander, R.E. Rogers, RSC Adv. **5**(76), 61508 (2015)
4. Ihsanullah, A. Abbas, A.M. Al-Amer, T. Laoui, M.J. Al-Marri, M.S. Nasser, M. Khraisheh, M.A. Atieh, Sep. Purif. Technol. **157**, 141 (2016)
5. W. Li, A. Dichiaro, J. Bai, Compos. Sci. Technol. **74**, 221 (2013)
6. G. Mittal, V. Dhand, K.Y. Rhee, S.J. Park, W.R. Lee, J. Ind. Eng. Chem. **21**, 11 (2015)
7. V. Jourdain, C. Bichara, Carbon **58**, 2 (2013)
8. R. Guzmán de Villoria, A.J. Hart, B.L. Wardle, ACS Nano **5**(6), 4850 (2011)
9. T. Yamada, A. Maigne, M. Yudasaka, K. Mizuno, D.N. Futaba, M. Yumura, S. Iijima, K. Hata, Nano Lett. **8**(12), 4288 (2008)
10. A. Moissala, A.G. Nasibulin, E.I. Kauppinen, J. Phys. Condens. Matter **15**(42), S3011 (2003)
11. C. Castro, M. Pinault, S. Coste-Leconte, D. Porterat, N. Bendiab, C. Reynaud, M. Mayne-L'Hermite, Carbon **48**(13), 3807 (2010)
12. Q. Zhang, J.Q. Huang, M.Q. Zhao, W.Z. Qian, F. Wei, Appl. Phys. A Mater. Sci. Process. **94**(4), 853 (2009)
13. C. Castro, M. Pinault, D. Porterat, C. Reynaud, M. Mayne-L'Hermite, Carbon **61**, 585 (2013)
14. C.L. Cheung, A. Kurtz, H. Park, C.M. Lieber, J. Phys. Chem. B **106**(10), 2429 (2002)
15. R. Rao, D. Liptak, T. Cherukuri, B.I. Yakobson, B. Maruyama, Nat. Mater. **11**(3), 213 (2012)
16. Y. Liu, A. Dobrinsky, B.I. Yakobson, Phys. Rev. Lett. **105**(23), 235502 (2010)
17. R.L.V. Wal, D.L. Dietrich, Appl. Opt. **34**(6), 1103 (1995)
18. R.W. Weeks, W.W. Duley, J. Appl. Phys. **45**(10), 4661 (1974)
19. A.C. Eckbreth, J. Appl. Phys. **48**(11), 4473 (1977)
20. L.A. Melton, Appl. Opt. **23**(13), 2201 (1984)
21. P. Roth, A. Filippov, J. Aerosol Sci. **27**(1), 95 (1996)
22. A. Filippov, M. Markus, P. Roth, J. Aerosol Sci. **30**(1), 71 (1999)
23. S. Will, S. Schraml, A. Leipertz, Opt. Lett. **20**(22), 2342 (1995)
24. R.L. Vander Wal, M.Y. Choi, Carbon **37**(2), 231 (1999)
25. B. Axelsson, R. Collin, P.E. Bengtsson, Appl. Opt. **39**(21), 3683 (2000)
26. H. Bladh, P.E. Bengtsson, Appl. Phys. B **78**(2), 241 (2004)
27. D. Snelling, K. Thomson, F. Liu, G. Smallwood, Appl. Phys. B **96**(4), 657 (2009)
28. H.A. Michelsen, P.O. Witze, D. Kayes, S. Hochgreb, Appl. Opt. **42**(27), 5577 (2003)
29. H.A. Michelsen, J. Chem. Phys. **118**(15), 7012 (2003)
30. S. Dankers, A. Leipertz, S. Will, J. Arndt, K. Vogel, S. Schraml, A. Hemm, Chem. Eng. Technol. **26**(9), 966 (2003)
31. R.L. Vander Wal, G.M. Berger, T.M. Tichich, P.D. Patel, Appl. Opt. **41**(27), 5678 (2002)
32. D.R. Snelling, G.J. Smallwood, F. Liu, Ö.L. Gülder, W.D. Bachalo, Appl. Opt. **44**(31), 6773 (2005)
33. B.F. Kock, B. Tribalet, C. Schulz, P. Roth, Combust. Flame **147**(1–2), 79 (2006)
34. A. Leipertz, S. Dankers, Part. Part. Syst. Charact. **20**(2), 81 (2003)
35. Y. Murakami, T. Sugatani, Y. Nosaka, J. Phys. Chem. A **109**(40), 8994 (2005)
36. T. Sipkens, G. Joshi, K. Daun, Y. Murakami, J. Heat Transf. **135**(5), 052401 (2013)
37. A. Eremin, E. Gurentsov, Appl. Phys. A **119**(2), 615 (2015)
38. L. Landström, P. Heszler, J. Phys. Chem. B **108**(20), 6216 (2004)
39. R.L. Vander Wal, T.M. Tichich, J.R. West, Appl. Opt. **38**(27), 5867 (1999)
40. R. Starke, B. Kock, P. Roth, Shock Waves **12**(5), 351 (2003)
41. A. Eremin, E. Gurentsov, C. Schulz, J. Phys. D Appl. Phys. **41**(5), 055203 (2008)
42. A. Eremin, E. Gurentsov, E. Popova, K. Priemchenko, Appl. Phys. B **104**(2), 285 (2011)
43. B.F. Kock, C. Kayan, J. Knipping, H.R. Orthner, P. Roth, Proc. Combust. Inst. **30**(1), 1689 (2005)
44. A. Eremin, E. Gurentsov, E. Mikheyeva, K. Priemchenko, Appl. Phys. B **112**(3), 421 (2013)
45. T. Sipkens, N. Singh, K. Daun, N. Bizmark, M. Ioannidis, Appl. Phys. B **119**(4), 561 (2015)
46. L. Landström, K. Elihn, M. Boman, C. Granqvist, P. Heszler, Appl. Phys. A **81**(4), 827 (2005)
47. J. Knipping, H. Wiggers, B. Kock, T. Hülser, B. Rellinghaus, P. Roth, Nanotechnology **15**(11), 1665 (2004)
48. A.V. Eremin, E.V. Gurentsov, S.A. Musikhin, Mater. Res. Express **3**(10), 105041 (2016)
49. A. Eremin, E. Gurentsov, S. Musikhin, J. Alloys Compd **727**, 711 (2017)
50. E. Cenko, G. Bruneaux, L. Pickett, C. Schulz, SAE Int. J. Eng. **6**(1), 352 (2013)
51. R. Ryser, T. Gerber, T. Dreier, Combust. Flame **156**(1), 120 (2009)
52. B. Bougie, M. Tulej, T. Dreier, N. Dam, J. Ter Meulen, T. Gerber, Appl. Phys. B **80**(8), 1039 (2005)
53. H. Oltmann, J. Reimann, S. Will, Combust. Flame **157**(3), 516 (2010)
54. T.D. Durbin, K. Johnson, D.R. Cocker, J.W. Miller, H. Maldonado, A. Shah, C. Ensfield, C. Weaver, M. Akard, N. Harvey et al., Environ. Sci. Technol. **41**(17), 6199 (2007)
55. G.J. Smallwood, D. Clavel, D. Gareau, R.A. Sawchuk, D.R. Snelling, P.O. Witze, B. Axelsson, W.D. Bachalo, Ö.L. Gülder, SAE Trans. **111**, 1345–1360 (2002)
56. M. Johnson, M. Hilton, D. Waterman, J. Black, Meas. Sci. Technol. **14**(7), 1146 (2003)
57. P.O. Witze, SAE Trans. **111**, 661–672 (2002)
58. J.D. Black, M. Hilton, M.P. Johnson, D. Waterman, in *Laser Applications in Medicine, Biology, and Environmental Science*, vol. 5149 (International Society for Optics and Photonics, 2003), pp. 265–273
59. M. Cau, N. Dorval, B. Attal-Trétout, J.L. Cochon, A. Foutel-Richard, A. Loiseau, V. Krüger, M. Tsurikov, C.D. Scott, Phys. Rev. B **81**, 165416 (2010)
60. S. Yatom, J. Bak, A. Khrabryi, Y. Raitses, Carbon **117**, 154 (2017)

61. Y. Xu, Y. Ma, Y. Liu, S. Feng, D. He, P. Haghi-Ashtiani, A. Dichiara, L. Zimmer, J. Bai, *J. Phys. Chem. C* **122**(11), 6437 (2018)
62. B. Satishkumar, A. Govindaraj, R. Sen, C. Rao, *Chem. Phys. Lett.* **293**(1), 47 (1998)
63. R. Xiang, E. Einarsson, J. Okawa, Y. Miyauchi, S. Maruyama, *J. Phys. Chem. C* **113**(18), 7511 (2009)
64. D. He, M. Bozlar, M. Genestoux, J. Bai, *Carbon* **48**(4), 1159 (2010)
65. A. Dichiara, J. Bai, *Diam. Relat. Mater.* **29**, 52 (2012)
66. D.W. Marquardt, *J. Soc. Ind. Appl. Math.* **11**(2), 431 (1963)
67. E.V. Gurentsov, A.V. Eremin, *High Temp.* **49**(5), 667 (2011)
68. E. Gurentsov, A. Eremin, P. Roth, R. Starke, *Kinet. Catal.* **46**(3), 309 (2005)
69. I.M. Sobol, *Math. Model. Comput. Exp.* **1**(4), 407 (1993)
70. I.M. Sobol, *Math. Comput. Simul.* **55**(1–3), 271 (2001)
71. J. Nossent, P. Elsen, W. Bauwens, *Environ. Model. Softw.* **26**(12), 1515 (2011)
72. G. Glen, K. Isaacs, *Environ. Model. Softw.* **37**, 157 (2012)
73. K. Kuwana, K. Saito, *Proc. Combust. Inst.* **31**(2), 1857 (2007)
74. D. Conroy, A. Moisala, S. Cardoso, A. Windle, J. Davidson, *Chem. Eng. Sci.* **65**(10), 2965 (2010)
75. S. Futko, B. Shulitskii, V. Labunov, E. Ermolaeva, *J. Eng. Phys. Thermophys.* **88**(6), 1432 (2015)
76. Y. Ma, A.B. Dichiara, D. He, L. Zimmer, J. Bai, *Carbon* **107**, 171 (2016)
77. P. Ho, M.E. Coltrin, W.G. Breiland, *J. Phys. Chem.* **98**(40), 10138 (1994)
78. Y. Nozaki, K. Kongo, T. Miyazaki, M. Kitazoe, K. Horii, H. Umemoto, A. Masuda, H. Matsumura, *J. Appl. Phys.* **88**(9), 5437 (2000)
79. C. Kaminski, P. Ewart, *Appl. Phys. B* **61**(6), 585 (1995)
80. S. Yatom, A. Khrabry, J. Mitrani, A. Khodak, I. Kaganovich, V. Vekselman, B. Stratton, Y. Raitzes, *MRS Commun.* **8**(3), 842 (2018)

Publisher's Note Springer Nature remains neutral with regard to jurisdictional claims in published maps and institutional affiliations.